

Supplementary Information

Sr₂Fe_{1.5-x}Mn_{0.1}Mo_{0.5}O_{6-δ} perovskite cathode for highly efficient CO₂ electrolysis

Yunan Jiang, Yang Yi, Changrong Xia,^{a*} and Henny J.M. Bouwmeester^{ab*}

^a CAS Key Laboratory of Materials for Energy Conversion Department of Materials Science and Engineering, University of Science and Technology of China, No. 96 Jinzhai Road, Hefei, Anhui Province, 230026, P.R. China. Email: xiacr@ustc.edu.cn

^b Electrochemistry Research Group, Membrane Science and Technology, Department of Science and Technology, MESA+ Research Institute for Nanotechnology, University of Twente, Drienerlolaan 5, 7522 NB Enschede, The Netherlands. E-mail: h.j.m.bouwmeester@utwente.nl

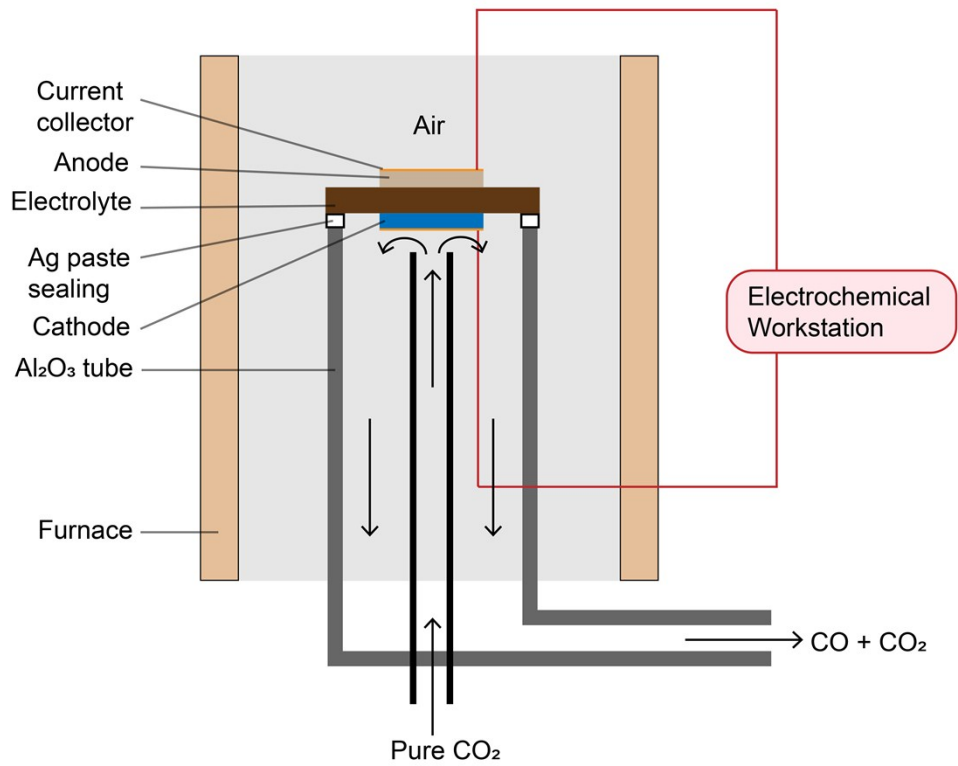


Fig. S1 Schematics of the electrochemical cell and experimental set-up used for CO₂ electrolysis tests.

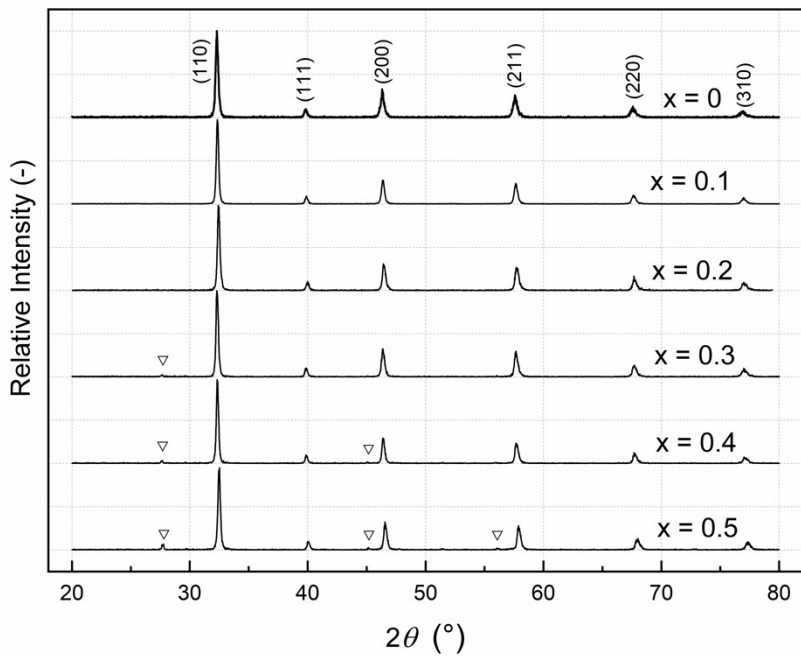


Fig. S2 Room temperature X-ray powder diffraction patterns of as-synthesized SFMMx ($x = 0 - 0.5$). The triangles (∇) denote the presence of SrMoO₄ impurity phase.

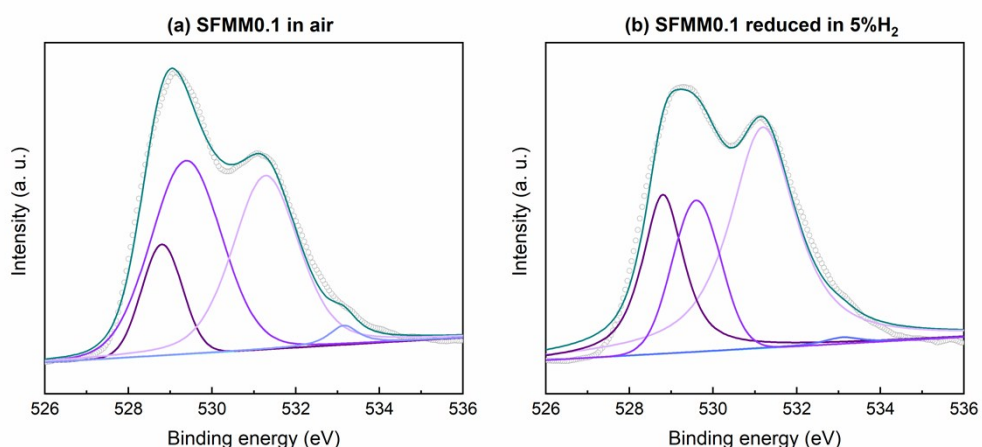


Fig. S3 Experimental and deconvoluted O1s XPS spectra for SFMM0.1 (a) as-synthesized at 1100 °C in air, and (b) after reduction at 850 °C in 5%H₂/Ar. The assignment of peaks in the O1s spectra of oxides is subject to significant controversy in literature. Peaks in the lower binding energy (BE) range are usually assigned to lattice oxygen, whereas the higher BE peaks are assigned to physisorbed oxygen (at medium BE) or oxygen in OH radicals, H₂O, CO or CO₂ (at the highest BE).

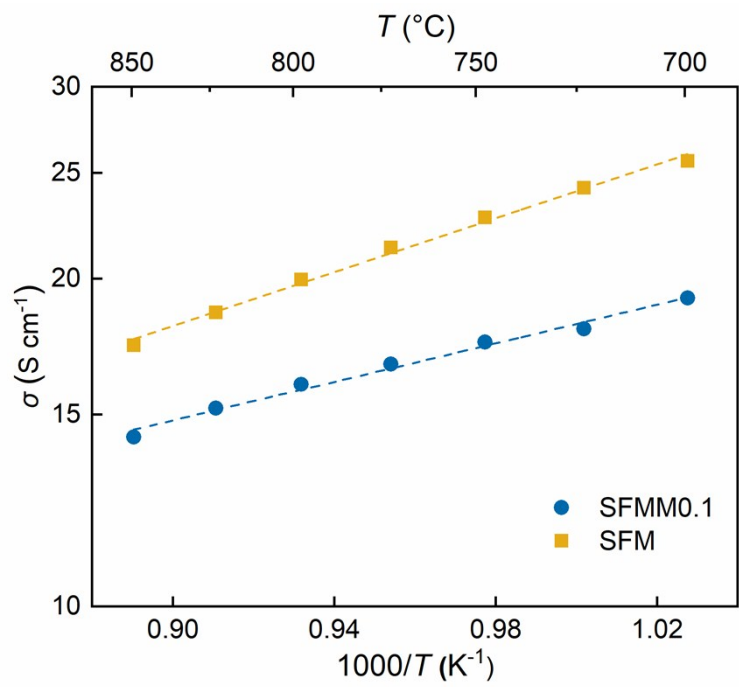


Fig. S4 Arrhenius plot of the total electrical conductivity of SFM and SFMM0.1 in air.

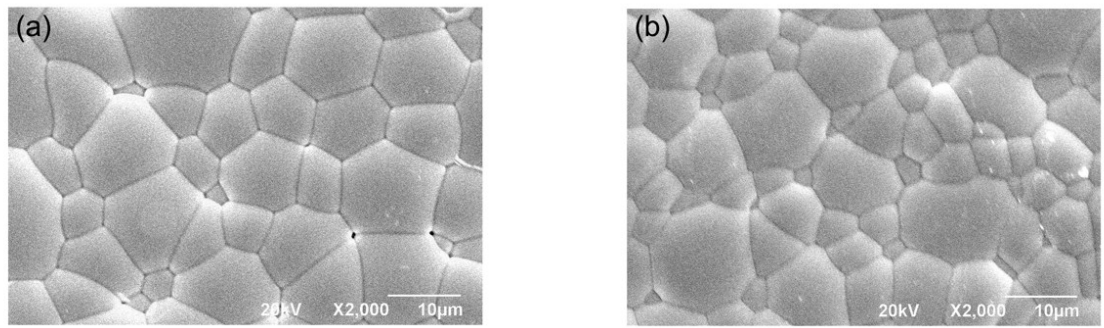


Fig. S5 SEM images of (a) SFM and (b) SFMM0.1 ceramic bars recorded after ECR experiments under CO/CO₂ conditions in the range 700 – 850 °C.

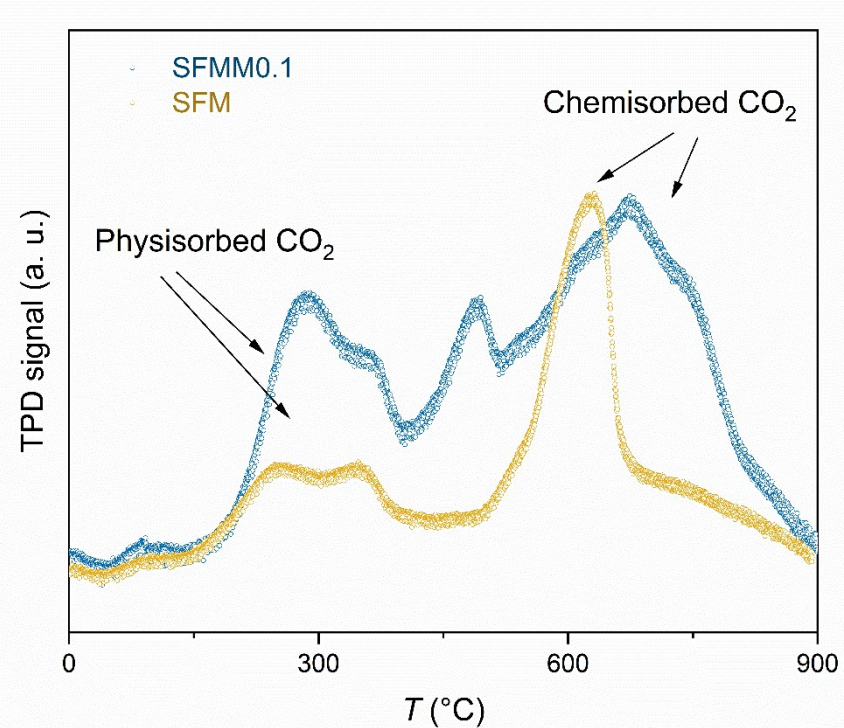


Fig. S6 TPD thermograms of CO_2 on SFM and SFMM0.1 powders. Comparatively high desorption rates observed at elevated temperature are attributed to desorption of chemisorbed CO_2 by contrast with the desorption of physisorbed CO_2 occurring at lower temperatures.

(a)

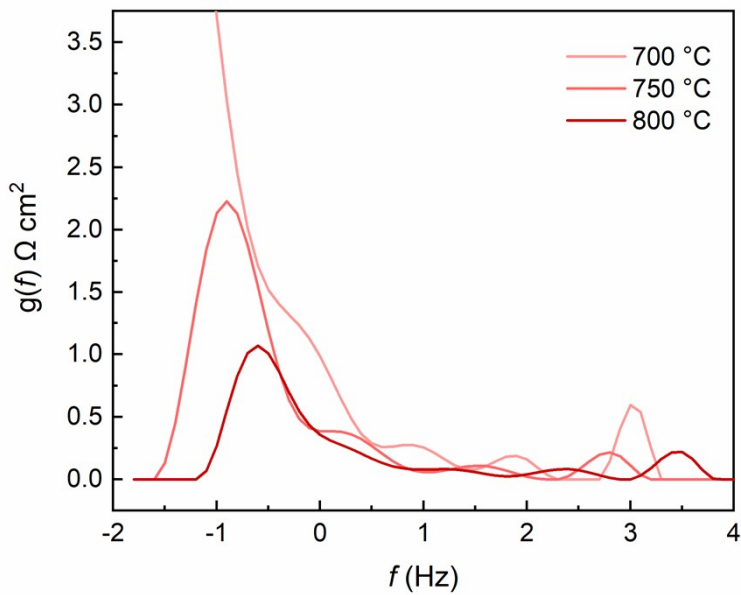
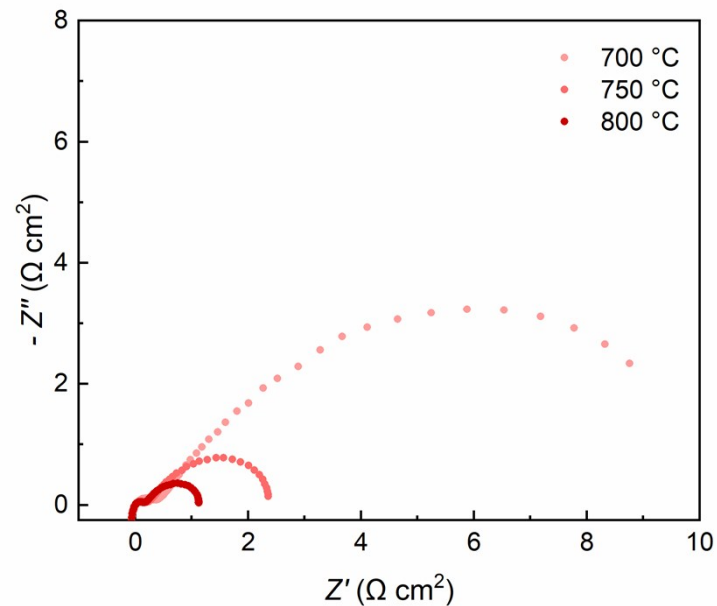


Fig. S7 (a) Impedance spectra and corresponding DRT plots of a symmetrical LSGM electrolyte-supported cell with SFM electrodes. The impedance spectra are shown after subtraction of the apparent electrolyte resistance.

(b)

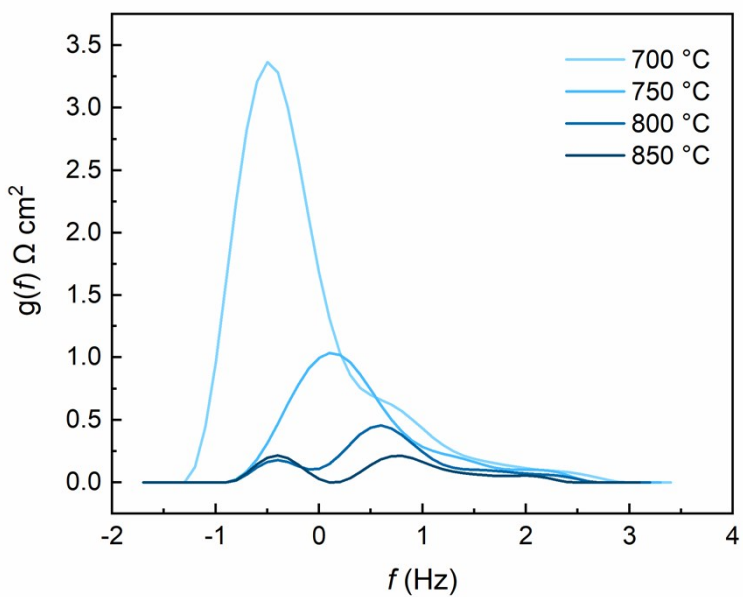
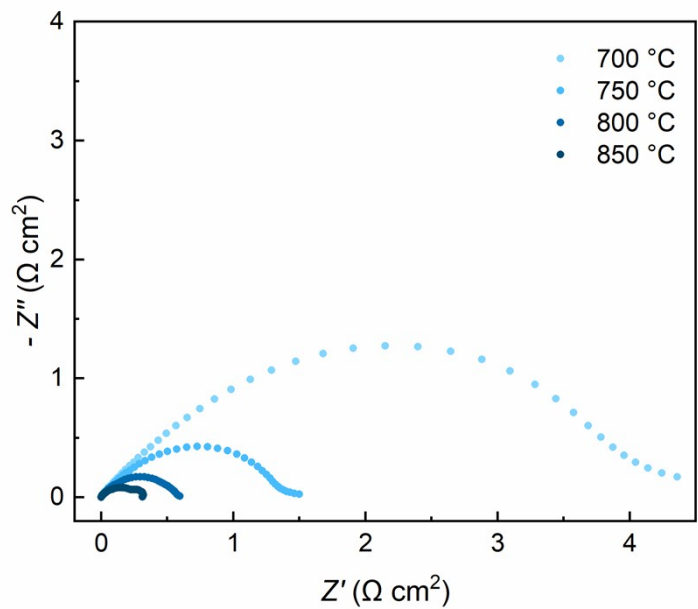


Fig. S7 (Contd.) (b) Impedance spectra and corresponding DRT plots of a symmetrical LSGM electrolyte-supported cell with SFMM0.1electrodes. The impedance spectra are shown after subtraction of the apparent electrolyte resistance.

(c)

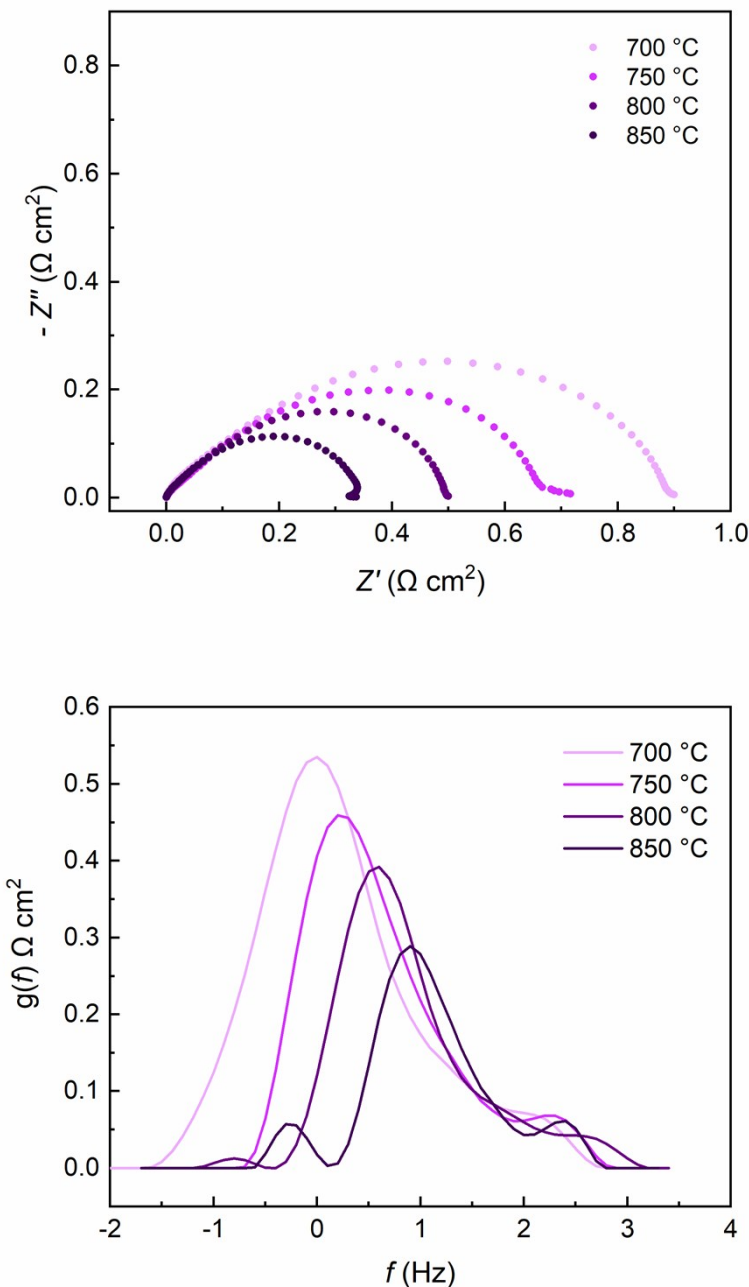


Fig. S7 (Contd.) (c) Impedance spectra and corresponding DRT plots of a symmetrical LSGM electrolyte-supported cell with SFMM0.1-SDC electrodes. The impedance spectra are shown after subtraction of the apparent electrolyte resistance.

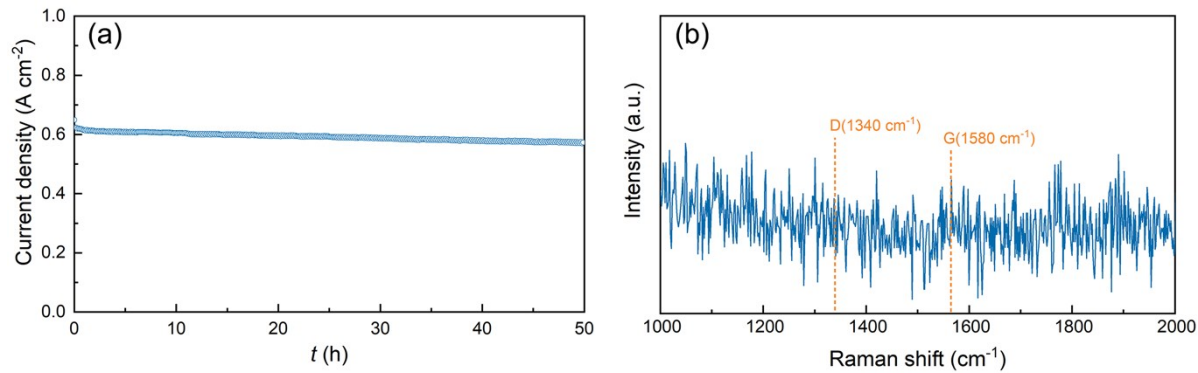


Fig. S8 (a) Short-term stability test of the cell operated in CO_2 electrolysis mode under a constant voltage load of 1.3 V and (b) Raman spectrum of the fuel electrode recorded after testing. The D-band at 1340 cm^{-1} and G-band at 1580 cm^{-1} are characteristic bands in the Raman spectra of graphitic materials.

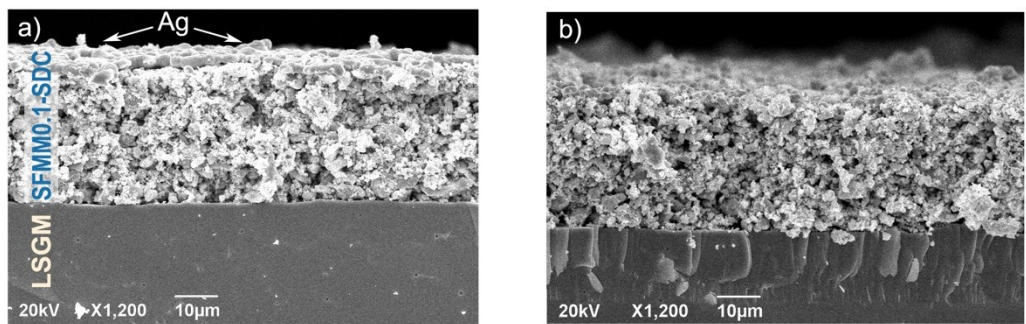


Fig. S9 SEM images of the SFMMn0.1-SDC | LSGM | LSCF-SDC cell recorded (a) before and (b) after 50 h CO_2 electrolysis operation at 750 $^{\circ}\text{C}$.

Table S1. Lattice parameters and reliability factors obtained from Rietveld refinements of room temperature X-ray powder diffraction patterns of SFMM0.1 as-synthesized at 1100 °C in air (oxidized) and after reduction at 850 °C in 5% H₂/Ar (reduced).

	Space group	<i>a</i> [Å]	ωR_p [%]	<i>R</i> _p [%]	χ^2
Oxidized	<i>Fm</i> 3 <i>m</i>	7.84176(4)	7.65	5.97	3.333
Reduced	<i>Fm</i> 3 <i>m</i>	7.86728(4)	8.08	5.99	3.564

Table S2. Average oxidation state of the B-site elements in SFMM0.1 as-synthesized at 1100 °C in air (oxidized) and after reduction at 850 °C in 5% H₂/Ar (reduced). Data were obtained from deconvolution of XPS spectra.

	Fe	Mn	Mo	average
Oxidized	+3.04	+2.70	+6.00	+3.76
Reduced	+2.92	+2.27	+5.90	+3.63

Table S3. Average Bader charges of atoms in stoichiometric SFMM0.1, non-stoichiometric SFMM0.1, *i.e.*, after removal of a neutral oxygen atom from a 2×2×2 supercell (Sr₈Fe₆Mo₂O₂₄), and difference value.

Element	Stoichiometric composition	Non-stoichiometric composition	Difference
Sr	+1.62	+1.59	-0.03
Fe	+1.69	+1.62	-0.07
Mn	+1.86	+1.67	-0.18
Mo	+2.49	+2.47	-0.02
O	-1.17	-1.19	+0.02

Table S4 Bond lengths and angles in adsorbed CO₂ on the perfect and oxygen-defective (Fe,Mo)O₂-terminated (100) surface of SFM and on the perfect and oxygen-defective (Fe,Mn,Mo)O₂-terminated (100) surface of SFMM0.25.

	Bond lengths			Bond angles		
	C-O1	C-O1	C-O1	∠O1-C-O2	∠O2-C-O3	∠O1-C-O3
	[Å]	[Å]	[Å]	[°]	[°]	[°]
SFM {Perfect}	1.27	1.27	1.37	131.2	114.3	114.5
SFM {oxygen-defective}	1.21	1.37	1.37	126.0	108.3	125.7
SFMM0.25 {perfect}	1.27	1.26	1.37	130.6	115.3	114.2
SFMM0.25 {oxygen-defective}	1.21	1.37	1.37	125.9	108.3	125.7

Table S5. Polarization resistance (R_p) of SFM, SFMM0.1 and SFMM0.1-SDC electrodes. Data were extracted from impedance spectra of symmetrical LSGM electrolyte-supported cells obtained under open circuit conditions in 50% CO/CO₂ at different temperatures. Data given for SFM were taken from our previous study.¹

	700 °C	750 °C	800 °C	850 °C
	[Ω cm ²]			
SFM	8.76	2.36	1.12	-
SFMM0.1	4.36	1.50	0.60	0.31
SFMM0.1-SDC	0.90	0.71	0.50	0.34

Table S6. Performance of Ni/YSZ cathodes for CO₂ reduction in solid oxide electrolysis cells at specified cell voltage (*V*) and specified temperature (*T*).

Gas composition	Current density [A cm ⁻²]	<i>V</i> [V]	<i>T</i> [°]	Ref.
50% CO/CO ₂	0.65	1.2	850	2
30% CO/CO ₂	0.80	1.2	850	2
25% CO/50% CO ₂ /Ar	0.77	1.2	850	3
25% H ₂ /CO ₂	0.90	1.2	800	4
50% CO/CO ₂	0.75	1.2	850	5
25% H ₂ /CO ₂	0.91	1.2	800	6
50% CO/CO ₂	0.34	1.5	900	7
30% CO/CO ₂	0.28	1.5	900	7
30% CO/CO ₂	1.37	1.5	800	8

Table S7. Performance of perovskite-type oxides with exsolved metal or alloy particles as cathode for CO₂ reduction in solid oxide electrolysis cells at specified cell voltage (*V*) and temperature (*T*). In a few cases, also the performance of the perovskite oxide host lattice is indicated.

Electrode	Gas composition	Current density [A cm ⁻²]	<i>V</i> [V]	<i>T</i> [°]	Ref.
Cu@($\text{La}_{0.75}\text{Sr}_{0.25}$) _{0.9} (Cr _{0.5} Mn _{0.5}) _{0.9} Cu _{0.1} O _{3-δ} -SDC	CO ₂	0.23	1.5	800	9
$\text{La}_{0.75}\text{Sr}_{0.25}\text{Cr}_{0.5}\text{Mn}_{0.5}\text{O}_{3-δ}$ -SDC	CO ₂	0.14	1.5	800	9
Ni@($\text{La}_{0.2}\text{Sr}_{0.8}$) _{0.9} (Ti _{0.8} Mn _{0.1}) _{0.9} Ni _{0.1} O _{3-δ} -YSZ	CO ₂	0.08	1.5	800	10
$\text{La}_{0.2}\text{Sr}_{0.8}\text{Ti}_{0.8}\text{Mn}_{0.1}\text{O}_{3-δ}$ -YSZ	1% CO/50% CO ₂ /Ar	0.05	1.5	800	10
Ni@($\text{La}_{0.75}\text{Sr}_{0.25}$) _{0.9} (Cr _{0.5} Mn _{0.5}) _{0.9} Ni _{0.1} O _{3-δ} -SDC	50% CO/CO ₂	0.18	1.5	800	11
$\text{La}_{0.75}\text{Sr}_{0.25}\text{Cr}_{0.5}\text{Mn}_{0.5}\text{O}_{3-δ}$ -SDC	CO ₂	0.14	1.5	800	11
NiFe@ $\text{La}_{0.6}\text{Sr}_{0.4}\text{Fe}_{0.8}\text{Mn}_{0.2}\text{O}_{3-δ}$	1% CO/50% CO ₂ /Ar	1.68	1.5	800	12
NiFe@ $\text{La}_{0.6}\text{Sr}_{0.4}\text{Fe}_{0.8}\text{Ni}_{0.2}\text{O}_{3-δ}$ -GDC	30% CO/CO ₂	0.60	1.5	800	13
NiFe@ $\text{La}_{0.6}\text{Sr}_{0.4}\text{Fe}_{0.8}\text{Ni}_{0.2}\text{O}_{3-δ}$ -GDC	CO ₂	0.65	1.5	800	14
FeCo@($\text{Pr}_{0.4}\text{Sr}_{0.6}$) ₃ (Fe _{0.85} Mo _{0.15}) ₂ O ₇	30% CO/CO ₂	0.87	1.5	850	15
$\text{Pr}_{0.4}\text{Sr}_{0.6}\text{Co}_{0.2}\text{Fe}_{0.7}\text{Mo}_{0.1}\text{O}_{3-δ}$	30% CO/CO ₂	0.68	1.5	850	15
Co@ $\text{PrBaMn}_{1.8}\text{Co}_{0.2}\text{O}_{5+δ}$	30% CO/CO ₂	0.78	1.5	800	16
Co@ $\text{La}_{0.6}\text{Sr}_{0.4}\text{Co}_{0.7}\text{Mn}_{0.3}\text{O}_{3-δ}$ -SDC	30% CO/CO ₂	0.80	1.5	800	17
NiFe@ $\text{La}_{0.6}\text{Ca}_{0.4}\text{Fe}_{0.8}\text{Ni}_{0.2}\text{O}_{3-δ}$ -SDC	CO ₂	0.80	1.5	800	18
NiFe@ $\text{Sr}_2\text{Fe}_{1.5}\text{Ni}_{0.1}\text{Mo}_{0.4}\text{O}_{6-δ}$ -SDC	CO ₂	2.16	1.5	800	19
NiFe ₃ @ $\text{Sr}_2\text{Fe}_{1.33}\text{Mo}_{0.45}\text{Ni}_{0.2}\text{O}_{6-δ}$ -GDC	CO ₂	0.93	1.6	800	20

References

- 1 Y. Li, B. Hu, C. Xia, W. Q. Xu, J. P. Lemmon and F. Chen, *J. Mater. Chem. A* 2017, **5**, 20833.
- 2 S. D. Ebbesen and M. Mogensen, *J. Power Sources*, 2009, **193**, 349.
- 3 S. D. Ebbesen, R. Knibbe and M. Mogensen, *J. Electrochem. Soc.*, 2012, **159**, F482.
- 4 Z. Zhan and L. Zhao, *J. Power Sources*, 2010, **195**, 7250.
- 5 C. Graves, S. D. Ebbesen and M. Mogensen, *Solid State Ionics*, 2011, **192**, 398.
- 6 Z. Zhan, W. Kobsiriphat, J. R. Wilson, M. Pillai, I. Kim and S. A. Barnett, *Energy & Fuels*, 2009, **23**, 3089.
- 7 X. Yue and J. T. S. Irvine, *Electrochem. Solid-State Lett.*, 2012, **15**, 31.
- 8 M. Zheng, S. Wang, Y. Yang and C. Xia, *J. Mater. Chem. A*, 2018, **6**, 2721.
- 9 H. Li, G. Sun, K. Xie, W. Qi, Q. Qin, H. Wei, S. Chen, Y. Wang, Y. Zhang and Y. Wu, *Int. J. Hydrogen Energy*, 2014, **39**, 20888.
- 10 Y. Li, K. Xie, S. Chen, H. Li, Y. Zhang and Y. Wu, *Electrochim. Acta*, 2015, **153**, 325.
- 11 C. Ruan and K. Xie, *Catal. Sci. & Technol.*, 2015, **5**, 1929.
- 12 S. Wang, H. Tsuruta, M. Asanuma, and T. Ishihara, *Adv. Energy Mater.*, 2015, **5**, 1401003
- 13 S. Liu, Q. Liu, and J.-L. Luo, *ACS Catalysis*, 2016, **6**, 6219.
- 14 Y. Tian, H. Zheng, L. Zhang, B. Chi and J. Pu, J. Li, *J. Electrochem. Soc.*, 2018, **165**, F17.
- 15 S. Liu, Q. Liu and J.-L. Luo, *J. Mater. Chem. A*, 2016, **4**, 17521.
- 16 Y. F. Sun, Y. Q. Zhang, J. Chen, J. H. Li, Y. T. Zhu, Y. M. Zeng, B. S. Amirkhiz, J. Li, B. Hua and J. L. Luo, *Nano Lett.*, 2016, **16**, 5303.
- 17 S. Park, Y. Kim, H. Han, Y. S. Chung, W. Yoon, J. Choi and W. B. Kim, *Appl. Catal. B: Environ.*, 2019, **248**, 147.
- 18 Y. Tian, L. Zhang, Y. Liu, L. Jia, J. Yang, C. Bo, J. Pu and J. Li, *J. Mater. Chem. A*, 2019, **7**, 6395
- 19 Y. Li, B. Hu, C. Xia, W. Q. Xu, J. P. Lemmon and F. Chen, *J. Mater. Chem. A*, 2017, **5**, 20833.
- 20 H. Lv, L. Le, X. Zhang, D. Gao, Y. Song, Y. Zhou, Q. Liu, G. Wang and X. Bao. *J. Mater. Chem. A*, 2019, **7**, 11967.